

Drell-Yan Lepton-Pair-Hadron Correlation in pA collisions

Anna Staśto,^{1,2,3,*} Bo-Wen Xiao,^{1,†} and David Zaslavsky^{1,‡}

¹*Department of Physics, Pennsylvania State University, University Park, PA 16802, USA*

²*RIKEN BNL Research Center, Building 510A, Brookhaven National Laboratory, Upton, NY 11973, USA*

³*H. Niewodniczański Institute of Nuclear Physics, Polish Academy of Sciences, Kraków, Poland*

In this paper, we numerically study the forward correlations between the lepton-pair and associated hadrons in Drell-Yan process in pA collisions. Using the present knowledge of the dipole gluon distribution from the modified Golec-Biernat-Wüsthoff model and from the solution of the Balitsky-Kovchegov evolution equation, we are able to compute and predict the forward correlations between the lepton-pair and associated hadron in Drell-Yan process at RHIC and LHC. Similar to the forward dihadron correlation in d–Au collisions measured at RHIC, the Drell-Yan type correlation also implies a strong suppression of the away side hadron at forward rapidity due to the strong interaction between the forward quark from the projectile proton and the gluon density from the target nucleus. Another feature of this process is that the correlation contains a double-peak structure in the away side, which makes it a unique observable.

I. INTRODUCTION

Over many years of both theoretical and experimental studies, Drell-Yan lepton pair production has been considered as one of the most interesting processes in high energy physics. Especially, single inclusive Drell-Yan lepton pair production in pA collisions is a cleaner probe than high- p_{\perp} hadrons since it has neither final state interactions nor fragmentation effects. Therefore, it provides a unique opportunity to study the parton distributions, especially the unintegrated gluon distributions [1–3], in hadrons. Furthermore, according to the high energy factorization, the hard photon-hadron and Drell-Yan lepton pair-hadron (virtual photon-hadron) correlations in pA collisions serve an important role in probing the low- x dipole gluon distributions.

In the small- x regime [4], there exist two distinct unintegrated gluon distributions, namely the Weizsäcker-Williams (WW) gluon distribution [5, 6] and the dipole gluon distribution [7]. According to its operator definition, the WW gluon distribution corresponds to the conventional gluon distribution, which measures the gluon density in the light-cone gauge. Although the dipole gluon distribution has no such interpretation, it is a fundamental quantity which appears in many processes involving hadrons. The dijet (or dihadron) correlations in DIS [8–10] can help us directly measure the WW gluon distribution which has never been explored experimentally before, while the Drell-Yan lepton-pair-hadron correlation can directly probe the dipole gluon distribution at small- x . Since the virtual photon does not interact with the gluons inside target hadrons, the final state effects are absent. As a result, this correlation can be calculated exactly in the leading order for all angles between the virtual photon and associated jet or hadron [10]. In contrast, due to the final state interactions, the so-called correlation limit or back-to-back limit has to be taken in order to arrive at a factorized formula for the dijet or dihadron processes.

Previous studies [11–17] of the Drell-Yan processes in pp or pA collisions have focused primarily on the inclusive cross sections, but not on the correlations between the outgoing hadron and the Drell-Yan lepton pair¹. As shown in Ref. [8–10], the correlations can reveal more dynamical information about the dense nuclear target and yield the direct measurement of the dipole gluon distribution.

The objective of this paper is to numerically study the correlations between the lepton-pair and associated hadron in the Drell-Yan process in pA collisions. This provides predictions for the correlations which can be measured at both RHIC and LHC [19].

To parametrize the dipole gluon distribution, we have employed two approaches. In the first one we used the Golec-Biernat-Wüsthoff (GBW) model [20] together with the geometrical scaling [21] which can successfully describe all the low- x DIS data. In deep inelastic scattering, the partonic cross section for a virtual photon scattering off a proton can

*Electronic address: astasto@phys.psu.edu

†Electronic address: bux10@psu.edu

‡Electronic address: dzaslavs@phys.psu.edu

¹ We also notice that there is a recent study[18] on the real prompt photon and hadron correlations in pA collisions. If we take the virtuality of the photon M^2 to be 0, and subtract the collinear divergence with proper scheme, we can also get the results for the real prompt photon and hadron correlations.

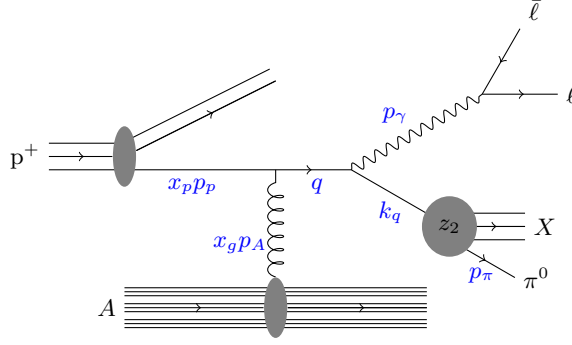


FIG. 1: The Drell-Yan scattering process, with several of the momentum variables used in our calculation labeled. p_p and p_A are respectively the momenta of the proton and the nucleus from which the gluon was emitted. p_γ is the momentum of the virtual photon as reconstructed from the lepton pair, and p_π is the measured momentum of the pion. x_p and x_g are the longitudinal momentum fractions of the quark relative to the proton and the gluon relative to the nucleon, $z = p_\gamma^+/q^+$ is the fraction of total momentum taken by the photon, and $z_2 = p_\pi^+/k_q^+$ is the fraction of the momentum of the quark jet that is carried by the pion.

be written in the color dipole model as a convolution of the photon wave function and the dipole-proton scattering amplitude. In the GBW model, the dipole scattering amplitude is parametrized as $S_{\text{GBW}}^{(2)}(r_\perp) = \exp\left[-\frac{r_\perp^2 Q_s^2}{4}\right]$ with r_\perp being the transverse size of the $q\bar{q}$ dipole. The geometrical scaling property means that if one writes $Q_s^2(x) = Q_{s0}^2(x/x_0)^{-\lambda}$ with $Q_{s0} = 1 \text{ GeV}$, $x_0 = 3.04 \times 10^{-3}$ and $\lambda = 0.288$ [22], the DIS total cross section only depends on one single variable $\tau = \frac{Q^2}{Q_s^2(x)}$, instead of the variables x and Q^2 separately. Although the geometric scaling was originally found in DIS on proton targets, it can be generalized to pA collisions as well [23]. One can write the saturation momentum scale Q_{sA} for target nuclei with mass number A as $Q_{sA}^2(x) = Q_{s0}^2 A^{\frac{1}{3}} c(b)(x/x_0)^{-\lambda}$, where $c(b)$ is the profile function which depends on the impact parameter b . This profile function is related to the centrality of the pA (or dA) collisions. Central collisions give large values of $c(b)$, while the peripheral collisions correspond to small values of the profile function.

In the second approach, we numerically solve the small- x evolution equation for the dipole amplitude, namely the Balitsky-Kovchegov (BK) equation [24, 25], using both fixed and running couplings. From these numerical solutions we then obtain the dipole gluon distribution in each case. We will discuss the implementation of this approach later in more detail.

Comparing to the dihadron (or dijet) correlations in pA processes, the Drell-Yan type correlation contains a unique feature on the away side. This correlation has a double-peak structure in the away side while other correlation functions exhibit a single peak structure. This difference comes from the fact that the dipole gluon distribution and the cross section both vanish when the transverse momentum of the gluon goes to zero. This leads to a vanishing partonic cross section when the produced virtual photon and quark are completely back-to-back. With the fragmentation effect which turns the quark into a pion (π^0), this effect gets smeared a little bit and becomes less visible. Nevertheless, taking into account the fragmentation, we find that the correlation has a minimum at $\Delta\phi = \pi$ and possesses a two-peak structure.

The rest of the paper is organized as follows. In Sec. II, we discuss the cross section of the Drell-Yan process with associated hadron in pA collisions and define the correlation function by dividing the single inclusive cross section of the DY process. We discuss the parametrization of the dipole gluon distributions in terms of different models in Sec. III. The numerical results and further discussions on the future experiments are given in Sec. IV. In Sec. V, we conclude and summarize.

II. DRELL-YAN LEPTON PAIR - HADRON CORRELATIONS

In the small- x regime, the Drell-Yan lepton pair production processes is dominated by the $qg \rightarrow q\gamma^*$ channel at the partonic level. Here the gluon g , in fact, can be regarded as a group of soft gluons from the dense nucleus target. The virtual photon then decays into a lepton pair and the quark fragments into a cluster of hadrons. We are interested in the correlation between the lepton pair and the hadron, say π^0 , which is a product of the fragmentation from the quark in the process $pA \rightarrow \ell\bar{\ell}\pi^0 X$. It is shown schematically in figure 1.

The cross section $\frac{d\sigma^{pA \rightarrow \ell\bar{\ell}\pi^0 X}}{d\mathcal{P} \cdot \mathcal{S}}$, which measures the probability of producing a virtual photon with an invariant

mass M and a quark with large p_\perp in the final state, has been calculated in [10] for the $pA \rightarrow \gamma^* qX$ channel. After summing over different photon polarizations, the total production cross section can be cast into²

$$\begin{aligned} \frac{d\sigma^{pA \rightarrow \gamma^* qX}}{dY_\gamma dY_q d^2\mathbf{p}_{\gamma\perp} d^2\mathbf{k}_{q\perp} d^2b} &= \sum_f x_p q_f(x_p, \mu) \frac{\alpha_{\text{em}} e_f^2}{2\pi^2} (1-z) F_{x_g}(q_\perp) \\ &\times \left\{ [1 + (1-z)^2] \frac{z^2 q_\perp^2}{[\tilde{P}_\perp^2 + \epsilon_M^2][(\tilde{\mathbf{P}}_\perp + z\mathbf{q}_\perp)^2 + \epsilon_M^2]} \right. \\ &\quad \left. - z^2(1-z)M^2 \left[\frac{1}{\tilde{P}_\perp^2 + \epsilon_M^2} - \frac{1}{(\tilde{\mathbf{P}}_\perp + z\mathbf{q}_\perp)^2 + \epsilon_M^2} \right]^2 \right\}, \quad (1) \end{aligned}$$

where $\epsilon_M^2 = (1-z)M^2$, $\mathbf{q}_\perp = \mathbf{p}_{\gamma\perp} + \mathbf{k}_{q\perp}$ and $\tilde{\mathbf{P}}_\perp = (1-z)\mathbf{p}_{\gamma\perp} - z\mathbf{k}_{q\perp}$. Here the normalized gluon distribution, $F_{x_g}(q_\perp) = \int \frac{d^2r_\perp}{(2\pi)^2} e^{-iq_\perp \cdot r_\perp} S_{x_g}^{(2)}(r_\perp)$, is defined through the Fourier transform of the dipole amplitude. It is straightforward to write down the corresponding cross section for the lepton pair production as follows

$$\frac{d\sigma^{pA \rightarrow l^+ l^- qX}}{dY_\gamma dY_q d^2\mathbf{p}_{\gamma\perp} d^2\mathbf{k}_{q\perp} d^2b d^2M^2} = \frac{\alpha_{\text{em}}}{3\pi M^2} \frac{d\sigma^{pA \rightarrow \gamma^* qX}}{dY_\gamma dY_q d^2\mathbf{p}_{\gamma\perp} d^2\mathbf{k}_{q\perp} d^2b}. \quad (2)$$

Therefore, one just needs to include a factor of $\frac{\alpha_{\text{em}}}{3\pi} \frac{dM^2}{M^2}$ to the photon cross sections to get the lepton pair cross sections. The factor $\frac{\alpha_{\text{em}}}{3\pi} \frac{1}{M^2}$ eventually cancels out in the correlation function (5).

To express the cross section in terms of the kinematic variables of the pion (π^0) and leptons, which are actually detected in the final state, we need to include in the above formula the fragmentation function of the quark into a pion, $D_{\pi^0/f}(z_2, \mu)$ to obtain

$$\begin{aligned} \frac{d\sigma^{pA \rightarrow \gamma^* \pi^0 X}}{dY_\gamma dY_\pi d^2\mathbf{p}_{\gamma\perp} d^2\mathbf{p}_{\pi\perp} d^2b} &= \int_{\frac{z_{h2}}{1-z_{h1}}}^1 \frac{dz_2}{z_2^2} \sum_f D_{\pi^0/f}(z_2, \mu) x_p q_f(x_p, \mu) \frac{\alpha_{\text{em}} e_f^2}{2\pi^2} (1-z) F_{x_g}(q_\perp) \\ &\times \left\{ [1 + (1-z)^2] \frac{z^2 q_\perp^2}{[\tilde{P}_\perp^2 + \epsilon_M^2][(\tilde{\mathbf{P}}_\perp + z\mathbf{q}_\perp)^2 + \epsilon_M^2]} \right. \\ &\quad \left. - z^2(1-z)M^2 \left[\frac{1}{\tilde{P}_\perp^2 + \epsilon_M^2} - \frac{1}{(\tilde{\mathbf{P}}_\perp + z\mathbf{q}_\perp)^2 + \epsilon_M^2} \right]^2 \right\}, \quad (3) \end{aligned}$$

where $z_{h1} \equiv p_\gamma^+/p_p^+$ and $z_{h2} \equiv p_\pi^+/p_p^+$ are the longitudinal momentum fraction of the virtual photon and final state π^0 hadron, respectively. μ^2 is the factorization scale which is set to be Q_{sA}^2 . The lower limit on the z_2 integral comes from requiring that $x_p < 1$.

The Drell-Yan lepton pair inclusive differential cross section can be obtained from the previous expression by integrating over the phase space of the final state quark, which makes it a function of the kinematic variables of the virtual photon only. By noting that $dY_\gamma dY_q = \frac{dz dx_p}{z(1-z)x_p}$, one can write the inclusive Drell-Yan cross section as

$$\begin{aligned} \frac{d\sigma^{pA \rightarrow \gamma^* X}}{dY_\gamma d^2\mathbf{p}_{\gamma\perp} d^2b} &= \int_{z_{h1}}^1 \frac{dz}{z} \iint d^2\mathbf{q}_\perp \sum_f x_p q_f(x_p, \mu) \frac{\alpha_{\text{em}} e_f^2}{2\pi^2} F_{x_g}(q_\perp) \\ &\times \left\{ [1 + (1-z)^2] \frac{z^2 q_\perp^2}{[p_{\gamma\perp}^2 + \epsilon_M^2][(\mathbf{p}_{\gamma\perp} - z\mathbf{q}_\perp)^2 + \epsilon_M^2]} \right. \\ &\quad \left. - z^2(1-z)M^2 \left[\frac{1}{p_{\gamma\perp}^2 + \epsilon_M^2} - \frac{1}{(\mathbf{p}_{\gamma\perp} - z\mathbf{q}_\perp)^2 + \epsilon_M^2} \right]^2 \right\}. \quad (4) \end{aligned}$$

² The rapidity is defined as respect to the center of mass frame of the scattering, which coincides with the lab frame when the energy of the proton projectile is the same as the energy per nucleon in the nucleus target.

This result is in agreement with the results in Ref. [12–15].

Integrating (3) and (4) over the magnitude of the transverse momenta with certain cutoff gives the cross sections as a function of rapidity and impact parameter only, $\frac{d\sigma^{pA \rightarrow \gamma^* \pi^0 X}}{dY_\gamma dY_\pi d^2\mathbf{b}}$ and $\frac{d\sigma^{pA \rightarrow \gamma^* X}}{dY_\gamma d^2\mathbf{b}}$. To set the lower limits on these momentum integrals, we impose a transverse momentum cutoff $p_{\perp \text{cut}}$ which can be set to match the experimental acceptance. The upper limits are again determined by requiring that the longitudinal momentum fraction of the initial quark x_p be less than 1. This would give the lower bound of z_2 integrals and upper bounds of momentum integrals. For the correlation measurement, either the virtual photon or the detected hadron can be the leading particle with larger transverse mass, while the other becomes the associated particle. In the code, we break the total contributions into two cases: (1) $\sqrt{p_{\gamma\perp}^2 + M^2} > p_{q\perp}$; (2) $\sqrt{p_{\gamma\perp}^2 + M^2} < p_{q\perp}$ which correspond to the region $z > \frac{1}{2}$ and $z < \frac{1}{2}$, respectively.

Finally, the ratio of these two cross sections defines the Drell-Yan pair-hadron correlation function $C^{\text{DY}}(\Delta\phi)$,

$$C^{\text{DY}}(\Delta\phi) = \frac{2\pi \int \cdots \int_{p_{\{\gamma, \pi\}\perp} > p_{\perp \text{cut}}} d\mathbf{p}_{\gamma\perp} d\mathbf{p}_{\pi\perp} \frac{d\sigma^{pA \rightarrow \gamma^* \pi^0 X}}{dY_\gamma dY_\pi d^2\mathbf{p}_{\gamma\perp} d^2\mathbf{p}_{\pi\perp} d^2b}}{\iint_{p_{\gamma\perp} > p_{\perp \text{cut}}} d^2\mathbf{p}_{\gamma\perp} \frac{d\sigma^{pA \rightarrow \gamma^* X}}{dY_\gamma d^2\mathbf{p}_{\gamma\perp} d^2b}}, \quad (5)$$

where $\Delta\phi$ is defined as the azimuthal angle difference between the virtual photon and measured π^0 . The correlation function expresses the probability density for a pion to be emitted at a specific azimuthal angle relative to the virtual photon (normally the rapidities of these two particles are chosen to be the same). When $\Delta\phi \simeq \pi$, that is, when the virtual photon and π^0 are almost back-to-back, the dominant contribution to the correlation function $C^{\text{DY}}(\Delta\phi)$ comes from the low q_\perp region of the gluon distribution $F_{x_g}(q_\perp)$. In contrast, the behavior of the correlation function $C^{\text{DY}}(\Delta\phi)$ at $\Delta\phi \simeq 0$ or 2π is mainly determined by the large transverse momentum part of the gluon distribution function $F_{x_g}(q_\perp)$.

In addition, as mentioned earlier, the partonic cross section vanishes at $q_\perp = 0$ as in Eq. (3). The physical interpretation is that the emission of the virtual photon from the quark requires that the quark gets a kick or an impulse in the transverse direction. Since the small- x gluons carry very little longitudinal momentum and the virtual photon does not interact with the dense small- x gluons from the target nucleus, the quark must change its transverse momentum during the multiple scattering with the gluons in order to radiate the photon. In other words, if the quark receives no impulse which change its momentum, the virtual photon will remain as part of the quark higher fock state wavefunction, and thus can not be produced in the final state. Due to this fact, we expect that $\Delta\phi = \pi$ should be a local minimum of the correlation function. Furthermore, there are two symmetrical maxima lying near $\Delta\phi = \pi$ as $q_\perp^2 F_{x_g}(q_\perp)$ increases with q_\perp and reaches its maximum at $q_\perp \simeq Q_s$. As a result, the correlation should have a unique double-peak structure on the away side. Note that the correlation function at $\Delta\phi = \pi$ is no longer zero due to the pion fragmentation function.

In terms of the numerical evaluation of the cross sections (3) and (4), we use the MSTW 2008 NLO parton distributions [26] for the parton distributions q_f and the DSS fragmentation functions [27] for the fragmentation functions $D_{\pi^0/q}$. In the case of the d-Au collisions at RHIC, since the parton distributions are only given for protons in Ref. [26], we obtain the parton distribution for neutrons by using the isospin symmetry, which gives $q_{u/p} = q_{d/n}$ and $q_{d/p} = q_{u/n}$.

III. THE DIPOLE GLUON DISTRIBUTION

The Drell-Yan cross section involves the so-called normalized dipole gluon distribution $F_{x_g}(q_\perp)$, which characterizes the dense gluon distribution in this process in the nucleus in the small- x regime. As discussed in Ref. [8], this function is related to the well-known dipole gluon distribution $xG^{(2)}$ as

$$xG^{(2)}(x, q_\perp) = \frac{N_c S_\perp}{2\pi^2 \alpha_s} q_\perp^2 F_{x_g}(q_\perp), \quad (6)$$

where S_\perp is the transverse area of the target nucleus, $N_c = 3$ is the number of colors, and α_s is the strong coupling constant.

As mentioned previously we have chosen two approaches to parametrize the normalized dipole gluon distribution $F_{x_g}(q_\perp)$, namely, the solution of the BK evolution equation [24, 25] and the GBW model [20]. F_{x_g} is a Fourier transform of the color dipole amplitude in the coordinate space. The implementation of the solution to the leading

order BK equation for the phenomenological use is a little bit troublesome since it gives too fast energy evolution as compared to the experimental data from DIS. The GBW model describes the DIS data very well and is straightforward to use. However the GBW model fails to describe the proper behavior gluon distribution at large transverse momentum since it has an exponential drop off, while the perturbative QCD gives a result which drops in terms of powers of q_\perp . In practice, we use these two approaches for our numerical evaluation since they are complementary to each other. Our procedure is to fine-tune the behavior of the strong coupling constant α_s or the running coupling $\alpha_s(q)$ in the numerical solution of the BK equation until the solution has the same energy dependence and similar low q_\perp behavior as what the GBW model gives. Then we believe that the solution of the BK equation should be able to produce the correct large q_\perp part of the distribution and thus the correct angle correlation at $\Delta\phi = 0, 2\pi$.

A. The BK Equation

The Balitsky-Kovchegov (BK) equation governs the rapidity dependence of the color dipole scattering amplitude $\mathcal{N}(\mathbf{r}, \mathbf{b}, Y)$ [24, 25]. In position space, we can write the equation in terms of $S(\mathbf{r}, \mathbf{b}, Y) = 1 - \mathcal{N}(\mathbf{r}, \mathbf{b}, Y)$, as

$$\frac{\partial S(\mathbf{x} - \mathbf{y}, \mathbf{b}, Y)}{\partial Y} = -\bar{\alpha}_s \iint \frac{d^2 \mathbf{z}}{2\pi} \frac{(\mathbf{x} - \mathbf{y})^2}{(\mathbf{x} - \mathbf{z})^2 (\mathbf{z} - \mathbf{y})^2} \left[S(\mathbf{x} - \mathbf{y}, \mathbf{b}, Y) - S\left(\mathbf{x} - \mathbf{z}, \mathbf{b} + \frac{\mathbf{z} - \mathbf{y}}{2}, Y\right) S\left(\mathbf{z} - \mathbf{y}, \mathbf{b} + \frac{\mathbf{x} - \mathbf{z}}{2}, Y\right) \right]. \quad (7)$$

The above form of the equation is valid in the leading logarithmic order in $\ln 1/x$. One can also write the BK equation in terms of the momentum-space dipole scattering amplitude,

$$\phi(\mathbf{k}, Y) = \iint \frac{d^2 \mathbf{r}}{2\pi} e^{-i\mathbf{k} \cdot \mathbf{r}} \frac{N(\mathbf{r}, Y)}{r^2}. \quad (8)$$

As shown in Ref. [28], in terms of the function $\phi(\mathbf{k}, Y)$, the BK equation reads

$$\frac{\partial \phi(k, Y)}{\partial Y} = \bar{\alpha}_s K \otimes \phi(k) - \bar{\alpha}_s \phi^2(k), \quad (9)$$

where K represents the action of the BFKL kernel, which in the leading logarithmic approximation reads

$$K \otimes \phi(k) = \int_0^\infty \frac{dk'^2}{k'^2} \left[\frac{k'^2 \phi(k') - k^2 \phi(k)}{|k^2 - k'^2|} + \frac{k^2 \phi(k)}{\sqrt{4k'^4 + k^4}} \right]. \quad (10)$$

The Laplacian of ϕ is the function F_{x_g} that appears in the cross sections of section II.

$$F_{x_g}(\mathbf{k}, \mathbf{b}) = \frac{1}{2\pi} \nabla_{\mathbf{k}}^2 \phi(\mathbf{k}, \mathbf{b}, Y(x_g)) + \delta^2(\mathbf{k}). \quad (11)$$

Since the partonic cross section vanishes at $k = 0$, we can safely ignore the delta function in the above equation. Beyond this section, the \mathbf{b} dependence is left implicit.

The normalized dipole gluon distribution F_{x_g} at small x extracted from the solution to the leading order BK equation yields energy dependence which is too fast as compared with phenomenology. In addition, the numerical solution to the full NLO BK equation [29] is not yet ready for use in phenomenological study. In practice, we have chosen to modify the solution from the LO BK equation to obtain a realistic energy dependence by varying the behavior of the coupling constant. For a fixed coupling, we vary the value of the coupling constant directly; for the running coupling, we vary the value of Λ_{QCD} which controls the running behavior.

B. The Golec-Biernat Wusthoff Model

We can also parametrize the dipole gluon distributions by using the GBW model adapted for nuclear targets, which has both the nuclear enhancement and geometrical scaling [21, 30] feature. The geometrical scaling was found to be related to the traveling wave solutions [31–33] of the Balitsky-Kovchegov evolution.

For a dense proton target, the GBW model reads

$$\int d^2 \mathbf{b} \mathcal{N}(\mathbf{r}, \mathbf{b}, Y) = \mathcal{N}_0 (1 - e^{-r^2 Q_s^2/4}), \quad Q_s^2(Y) = Q_{s0}^2 x_0^\lambda e^{\lambda Y} = Q_{s0}^2 \left(\frac{x_0}{x} \right)^\lambda, \quad (12)$$

where $Q_{s0}^2 = 1 \text{ GeV}^2$, $\lambda = 0.288$ and $x_0 = 3.04 \times 10^{-4}$. As for a dense nuclear target with A nucleons inside, the saturation scale is subject to the nuclear enhancement which modifies the saturation momentum and gives $Q_{sA}^2(x) = Q_{s0}^2 A^{\frac{1}{3}} c(b)(x/x_0)^{-\lambda}$. Here the profile function $c(b)$ gives the centrality of the scattering. Using the GBW model, we can compute a simple analytic expression for F_{x_g} . According to equations (8) and (11) above, we get

$$\phi(k^2, Y) = \frac{1}{2} \Gamma\left(0, \frac{k^2}{Q_{sA}^2(Y)}\right), \quad (13)$$

$$F_{x_g}(k^2, Y) = \frac{1}{\pi Q_{sA}^2(Y)} e^{-k^2/Q_{sA}^2(Y)}, \quad (14)$$

where $\Gamma[0, x]$ is the incomplete gamma function.

C. The numerical solution of the BK equation

We solve the BK equation numerically [28] with initial condition for $\phi(k^2, Y)$ as in Eq. (13) at $Y_{\text{init}} = -\ln x_{\text{init}}$, where we use $x_{\text{init}} = 0.01$. This value is chosen to coincide with the upper applicable limit of the GBW model. With a solution for ϕ , using $F_{x_g}(k^2, Y) = \frac{1}{2\pi k^2} \frac{\partial^2 \phi(k^2, Y)}{\partial (\ln k)^2}$, we then compute F_{x_g} in the region $Y > Y_{\text{init}} = 4.6$ using a proper numerical differentiation scheme. The numerical solution to the BK equation for the gluon distribution is shown in figure 2 with fixed coupling, and in figure 4 for running coupling, as a function of the transverse momentum for different rapidities. For comparison also the analytic expression from the GBW model (14) is shown in figure 2. The BK solution possesses a larger tail in momentum as compared with the GBW model, which is due to the correct perturbative QCD limit.

1. Fixed Coupling

Since the solution to the leading order BK equation gives energy dependence which is too fast as compared to data (for inclusive DIS) if we use the normal value for α_s , we treat the strong coupling constant α_s as an adjustable parameter in the numerical computation. We need to find out the value of α_s which corresponds to the kinematic regime probed by these collisions in order to make meaningful predictions. Theoretically, the value of λ is predicted by various analytical approaches to the solution to the BK equation [31, 33]. The resulting saturation scale can be cast into

$$Q_s^2(Y) = \frac{Q_{s0}^2}{Y^{\frac{3}{2(1-\gamma_0)}}} \exp\left(-\frac{\bar{\alpha}_s \chi(\gamma_0)}{1-\gamma_0} Y\right), \quad (15)$$

where $\bar{\alpha}_s = \frac{\alpha_s N_c}{\pi}$, $\chi(\gamma)$ is the usual characteristic function the value of γ_0 is determined to be around 0.37. This function asymptotically approaches an exponential form,

$$Q_s^2(Y) \rightarrow C \exp(-\lambda Y), \quad \text{where } \lambda = \frac{\bar{\alpha}_s \chi(\gamma_0)}{1-\gamma_0} = \frac{4.88 N_c}{\pi} \alpha_s. \quad (16)$$

In terms of the numerical computation, as shown in figure 3, we extract the saturation scale from the output of the BK evolution and employ the procedure as described in Ref. [28], determining the value k_{max} of k which maximizes $k\phi(k^2, Y)$ at each Y , and set the saturation scale to be proportional to k_{max} . It is straightforward to show that the assumption $k_{\text{max}} \propto Q_s$ is valid for the GBW model. By matching the asymptotic behavior of the saturation momentum at large Y with the saturation momentum in the GBW model, we find that $\alpha_s \approx 0.062$ which is unusually small value for the strong coupling constant. Such small value of the strong coupling constant is an artifact of the large higher order corrections to the BK equation. If the higher order corrections and possibly resummation is included, the energy dependence extracted from the numerical solution of the BK equation should be close to the measured value with a reasonable value of α_s (see, e.g., in Ref. [34]).

With the fixed coupling, it seems that the BK evolution produces a transient spike in F_{x_g} at low k^2 , which is primarily due to our choice of the initial condition which differs substantially from the asymptotic solution at low k^2 . Given the fact that our code samples F_{x_g} within some extended region of q_{\perp}^2 for a certain value of $\Delta\phi$, this has very limited effect on our results.

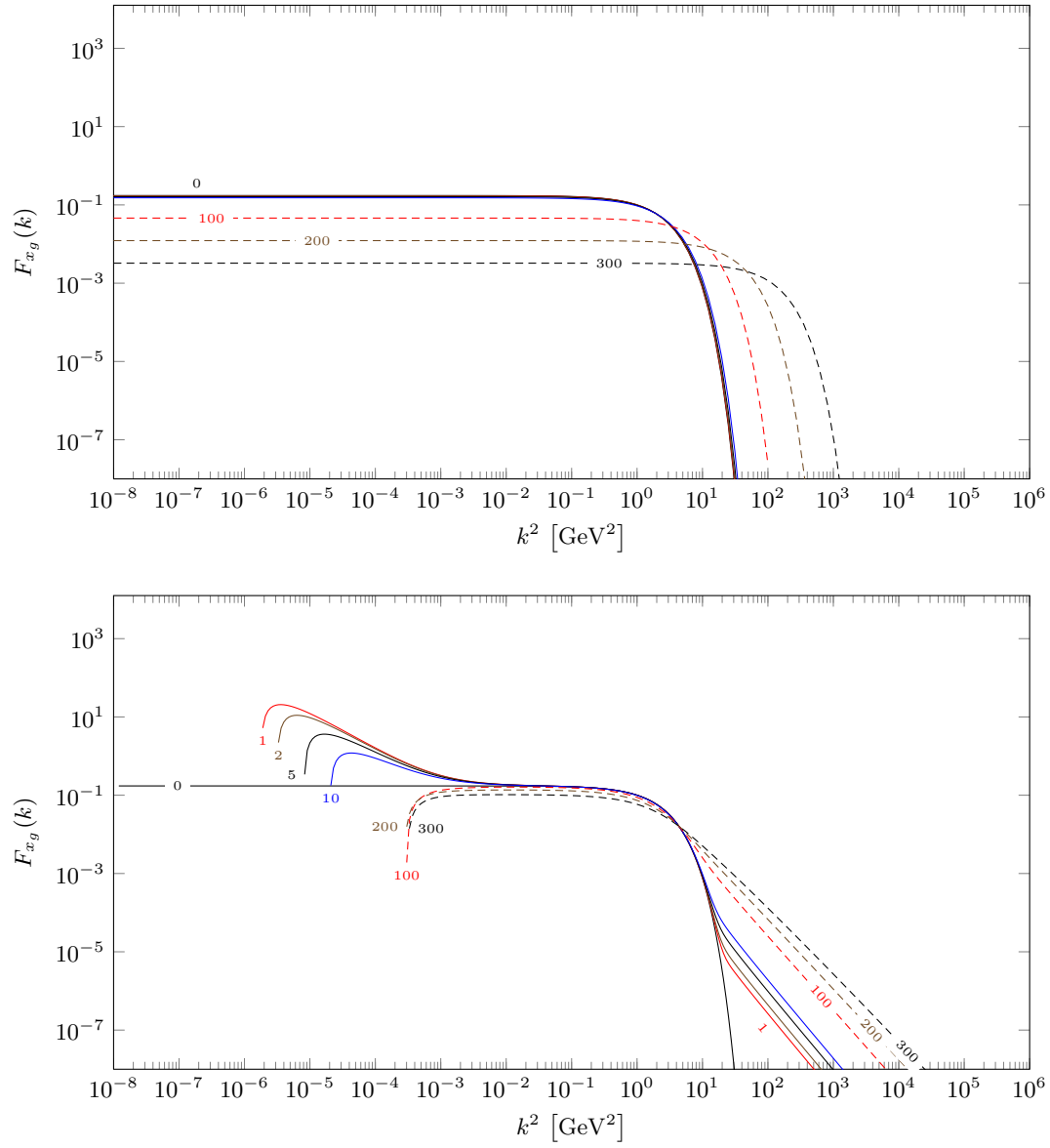


FIG. 2: The gluon distribution from the GBW model (14), on top, and the output of the numerical BK evolution with fixed coupling (11), on bottom, for central p-Pb collisions. Each curve shows $F_{x_g}(k)$ for $x_g = \exp(Y_{\text{init}} - n\delta Y)$, where n is the number that labels the curve and $\delta Y = \frac{1}{400} \ln(10^8) \approx 0.04605$ is the step size in rapidity used by the numerical integrator. The curve labeled 0 is the initial condition. Note the transient “spike” at the low k^2 region of the solution to the BK evolution, and the significant enhancement at large k^2 relative to the GBW model.

2. Running Coupling

Incorporating running coupling corrections into the leading order BK evolution is known to give a reasonably accurate description of DIS data [35, 36], and also to slow down the energy dependence of the saturation scale, which makes it a viable and perhaps preferable alternative to artificially tuning the value of α_s . In this case, the saturation scale dependence has also been calculated in [31] to be

$$Q_s^2(Y) \propto \Lambda_{\text{QCD}}^2 \exp \left(\sqrt{\frac{2\chi(\gamma_0)}{\beta(1-\gamma_0)}} Y + \frac{3}{4} \left(\frac{\chi''(\gamma_0)}{\sqrt{2\beta(1-\gamma_0)\chi(\gamma_0)}} \right)^{\frac{1}{3}} \xi_1 Y^{\frac{1}{6}} \right) \quad (17)$$

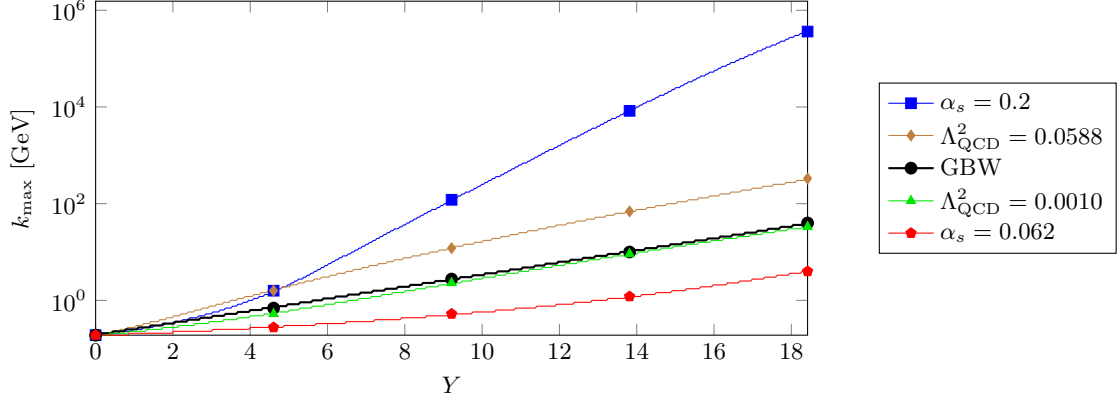


FIG. 3: This plot shows the peak of the momentum distribution, $k_{\max} = \max k\phi(k^2, Y)$, computed from the analytic formula for the GBW model, from the fixed coupling BK evolution for selected values of α_s , and from the running coupling BK evolution with selected values of Λ_{QCD}^2 . For the BK evolution curves, the slope in the upper range of rapidities decreases as α_s or Λ_{QCD}^2 decreases, and the closest match to the slope of the GBW model curve at $Y > 15$ is achieved with $\alpha_s = 0.062$ for fixed coupling or $\Lambda_{\text{QCD}}^2 = 0.001$ for running coupling. The jagged “steps” in the curves reflect the finite spacing of the momentum grid used in the evolution.

with a running coupling of the form

$$\bar{\alpha}_s(k^2) = \frac{1}{\beta \ln k^2 / \Lambda_{\text{QCD}}^2}, \quad (18)$$

where $\beta = \frac{11-2N_f/N_c}{12}$, $\xi_1 = -2.338\dots$ is the rightmost zero of the Airy function, $N_f = 3$ is the number of quark flavors that are expected to contribute, and $N_c = 3$ is the number of colors as before. Ref. [33] also includes a similar result.

However, this form is not practical for the numerical implementation due to a Landau pole at $k = \Lambda_{\text{QCD}}$. We use an implementation which shifts the squared momentum,

$$\bar{\alpha}_s(k^2) = \frac{1}{\beta \ln \frac{k^2 + \mu^2}{\Lambda_{\text{QCD}}^2}} \quad (19)$$

with $\mu = 1 \text{ GeV}$. The shift term μ^2 is a purely phenomenologically motivated change, which does not appear to significantly alter the behavior of $Q_s(Y)$ discussed below.

In equation (19), we are treating Λ_{QCD}^2 as an adjustable parameter which absorbs the free parameter $4C^2$ of Ref. [35]. We can alter the behavior of the coupling, and thus the energy dependence of the solution, by adjusting the value of Λ_{QCD}^2 . According to equation (17), the behavior of the saturation scale asymptotes to

$$Q_s \rightarrow e^{\lambda_r \sqrt{Y}}, \quad \text{where } \lambda_r = \sqrt{\frac{2\chi(\gamma_0)}{\beta(1-\gamma_0)}}. \quad (20)$$

This is qualitatively different from the large- Y behavior of the GBW model, thus it prevents us from reproducing the asymptotic behavior of that model. Nevertheless, we can choose a value of Λ_{QCD} that approximately matches $\frac{\partial Q_s}{\partial Y}$ to its value from the GBW model over the upper range of rapidities we calculate, $10 \lesssim Y \lesssim 20$. Some experimentation shows that $\Lambda_{\text{QCD}}^2 = 0.001 \text{ GeV}^2$ gives a reasonable match. The corresponding value from the fits in [35, 36] would be $\Lambda_{\text{QCD}}^2 \approx \frac{(0.241 \text{ GeV})^2}{4(6)} = 0.002 \text{ GeV}^2$, which is fairly close.

Note that the value of the effective Λ_{QCD} parameter determined by our fit is fairly small, which possibly indicates the need for further higher order corrections in the BK evolution (apart from the running coupling).

The solution we have obtained for the BK evolution with running coupling is shown in figure 4. Although the overall shapes of the curves are qualitatively similar, the evolution with rapidity is slowed by the running coupling. Overall, the actual value of F_{x_g} is less at large values of k^2 than it was in the fixed coupling case.

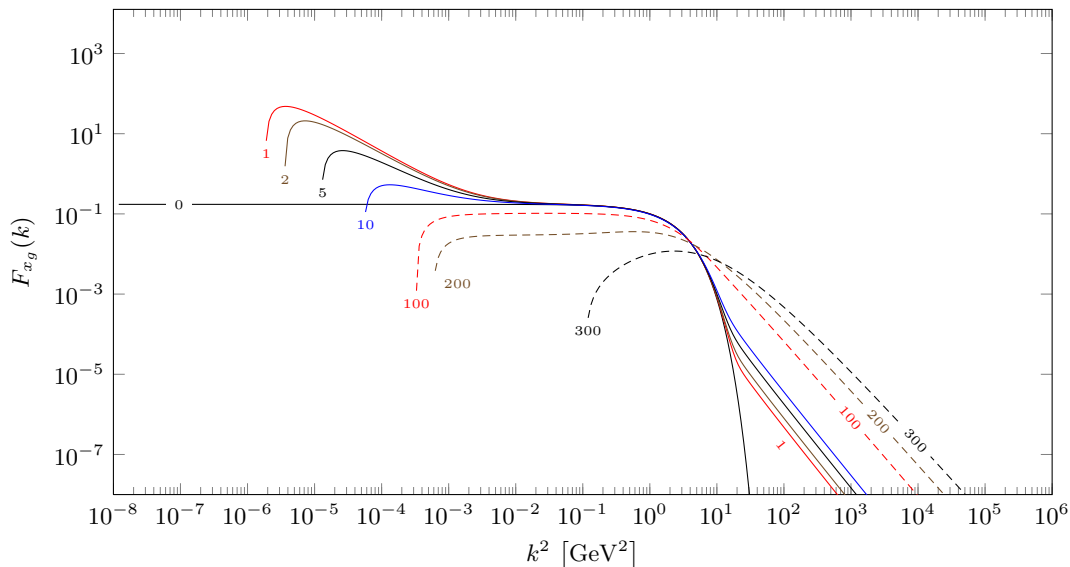


FIG. 4: The gluon distribution from the numerical BK evolution with the running coupling for central p-Pb collisions. This is a continuation of figure 2, and the labels have the same interpretation. As is well known, the running coupling slows down the evolution of the wavefront. Otherwise, the plots are similar to the fixed-coupling BK evolution, though there is some erratic behavior at lower momenta especially at high rapidities which was not seen to such a large extent in the fixed coupling case.

IV. RESULTS

With the gluon distribution determined from either the analytic GBW model and the numerical solution of the BK evolution described in section III, we can compute and study the correlation defined in section II. There are eight parameters involved in this calculation:

- the virtual photon mass M
- the photon and pion rapidities Y_γ and Y_π
- the profile function $c(b)$
- the mass number A
- the center-of-mass energy \sqrt{s} per nucleon
- the detector-imposed cutoff on the transverse momenta of the virtual photons or pions, $p_{\perp\text{cut}}$
- Different types of projectiles: either deuterons or protons.

To simulate results from d-Au collisions at RHIC, we set $\sqrt{s} = 200$ GeV, $A = 197$, and $p_{\perp\text{cut}} = 1.5$ GeV together with the use of the deuteron parton distribution functions. For LHC p-Pb collisions, we put $\sqrt{s} = 8800$ GeV which corresponds to the full design energy (14 TeV pp CM energy), $A = 208$, and $p_{\perp\text{cut}} = 3$ GeV. For both the RHIC and LHC measurement, we compute the correlation for a low and a high value of M . In addition, we set $Y_\gamma = Y_\pi$ which means that the virtual photons and pions are produced in the same rapidity window, and use $c(b) = 0.85$ which corresponds to central collisions.

We show our final results for the correlations in figures 5 and 6 with different specifically chosen parameters. From figs. 5 and 6, we find that indeed the GBW model and the BK equation with fixed and running couplings yield similar double-peak structure, as expected from our early discussion for the correlation function at the away side ($\Delta\phi \simeq \pi$). However, they differ dramatically at the near side ($\Delta\phi \simeq 0$ or 2π). It is easy to see that the near side correlation samples the large q_\perp region of the gluon distribution $F_{x_g}(q_\perp)$. Since this distribution is slightly greater with the running coupling than with fixed coupling, the near side peak is somewhat enhanced in the running coupling case.

We believe that the solution to the BK equation gives the correct large q_\perp behavior for the dipole gluon distribution while the GBW model fails at large q_\perp . Therefore, we expect that the curves generated by the numeric solution of the BK equation predicts the correlation for RHIC and LHC measurement for all azimuthal angle including both the near side and the away side.

V. CONCLUSION

In this paper, by using the GBW model and the numerical solution to the BK equation, we have numerically studied the correlations between the lepton-pair and associated hadron in Drell-Yan processes in pA collisions, which directly probe the dipole gluon distributions. The correlations have been computed for both RHIC d–Au collisions and LHC p–Pb collisions. We find that the Drell-Yan type correlation implies a strong suppression of the away side hadron at forward rapidity due to strong interaction between the forward quark from the projectile proton and the dense gluon from the target nucleus. In addition, we also emphasize that the Drell-Yan type correlation exhibits a unique double-peak structure in the away side.

Acknowledgments

We thank E. Avsar, F. Dominguez, A. Mueller and F. Yuan for helpful conversations. This work was supported in part by the U.S. Department of Energy under the contract DOE OJI grant No. DE - SC0002145 and by the Polish NCN grant DEC-2011/01/B/ST2/03915. AMS is supported by the Sloan Foundation. We are grateful to RIKEN, Brookhaven National Laboratory and the U.S. Department of Energy (contract number DE-AC02-98CH10886) for providing the facilities essential for the completion of this work.

-
- [1] S. Catani, M. Ciafaloni, F. Hautmann, Nucl. Phys. **B366**, 135-188 (1991).
 - [2] J. C. Collins, R. K. Ellis, Nucl. Phys. **B360**, 3-30 (1991).
 - [3] E. Avsar, arXiv:1203.1916 [hep-ph].
 - [4] E. Iancu, A. Leonidov and L. McLerran, arXiv:hep-ph/0202270; E. Iancu and R. Venugopalan, arXiv:hep-ph/0303204; J. Jalilian-Marian and Y. V. Kovchegov, Prog. Part. Nucl. Phys. **56**, 104 (2006) [arXiv:hep-ph/0505052]; F. Gelis, E. Iancu, J. Jalilian-Marian and R. Venugopalan, arXiv:1002.0333 [hep-ph]; and references therein.
 - [5] Y. V. Kovchegov and A. H. Mueller, Nucl. Phys. B **529**, 451 (1998) [arXiv:hep-ph/9802440].
 - [6] L. D. McLerran and R. Venugopalan, Phys. Rev. D **59**, 094002 (1999) [arXiv:hep-ph/9809427].
 - [7] D. Kharzeev, Y. V. Kovchegov and K. Tuchin, Phys. Rev. D **68**, 094013 (2003) [arXiv:hep-ph/0307037].
 - [8] F. Dominguez, B. W. Xiao and F. Yuan, Phys. Rev. Lett. **106**, 022301 (2011) [arXiv:1009.2141 [hep-ph]].
 - [9] F. Dominguez, C. Marquet, B. W. Xiao and F. Yuan, Phys. Rev. D **83**, 105005 (2011) [arXiv:1101.0715 [hep-ph]].
 - [10] F. Dominguez, J. -W. Qiu, B. -W. Xiao and F. Yuan, Phys. Rev. D **85**, 045003 (2012) [arXiv:1109.6293 [hep-ph]].
 - [11] J. C. Collins, D. E. Soper, G. F. Sterman, Nucl. Phys. **B250**, 199 (1985).
 - [12] B. Z. Kopeliovich, J. Raufeisen and A. V. Tarasov, Phys. Lett. B **503**, 91 (2001) [arXiv:hep-ph/0012035].
 - [13] R. Baier, A. H. Mueller and D. Schiff, Nucl. Phys. A **741**, 358 (2004) [arXiv:hep-ph/0403201].
 - [14] F. Gelis and J. Jalilian-Marian, Phys. Rev. D **67**, 074019 (2003) [arXiv:hep-ph/0211363].
 - [15] F. Gelis and J. Jalilian-Marian, Phys. Rev. D **66**, 094014 (2002) [arXiv:hep-ph/0208141].
 - [16] F. Gelis and J. Jalilian-Marian, Phys. Rev. D **76**, 074015 (2007) [arXiv:hep-ph/0609066].
 - [17] K. Golec-Biernat, E. Lewandowska and A. M. Stasto, Phys. Rev. D **82**, 094010 (2010) [arXiv:1008.2652 [hep-ph]].
 - [18] J. Jalilian-Marian and A. H. Rezaeian, arXiv:1204.1319 [hep-ph].
 - [19] C. A. Salgado, J. Alvarez-Muniz, F. Arleo, N. Armesto, M. Botje, M. Cacciari, J. Campbell and C. Carli *et al.*, J. Phys. G **39**, 015010 (2012) [arXiv:1105.3919 [hep-ph]].
 - [20] K. J. Golec-Biernat and M. Wusthoff, Phys. Rev. D **59**, 014017 (1998) [arXiv:hep-ph/9807513].
 - [21] A. M. Stasto, K. J. Golec-Biernat, J. Kwiecinski, Phys. Rev. Lett. **86**, 596-599 (2001) [arXiv:hep-ph/0007192].
 - [22] C. Marquet and L. Schoeffel, Phys. Lett. B **639**, 471 (2006) [arXiv:hep-ph/0606079].
 - [23] H. Kowalski, T. Lappi and R. Venugopalan, Phys. Rev. Lett. **100**, 022303 (2008) [arXiv:0705.3047 [hep-ph]].
 - [24] I. Balitsky, Nucl. Phys. B **463** (1996) 99 [arXiv:hep-ph/9509348]; Phys. Rev. Lett. **81** (1998) 2024 [arXiv:hep-ph/9807434]; Phys. Lett. B **518** (2001) 235 [arXiv:hep-ph/0105334].
 - [25] Y. V. Kovchegov, Phys. Rev. D **60** (1999) 034008 [arXiv:hep-ph/9901281]; Phys. Rev. D **61**, 074018 (2000) [arXiv:hep-ph/9905214].
 - [26] A. D. Martin, W. J. Stirling, R. S. Thorne and G. Watt, Eur. Phys. J. C **63**, 189 (2009) [arXiv:0901.0002 [hep-ph]].
 - [27] D. de Florian, R. Sassot and M. Stratmann, Phys. Rev. D **75**, 114010 (2007) [arXiv:hep-ph/0703242]; Phys. Rev. D **76**, 074033 (2007) [arXiv:0707.1506 [hep-ph]].
 - [28] K. J. Golec-Biernat, L. Motyka and A. M. Stasto, Phys. Rev. D **65**, 074037 (2002) [arXiv:hep-ph/0110325].
 - [29] E. Avsar, A. M. Stasto, D. N. Triantafyllopoulos and D. Zaslavsky, JHEP **1110**, 138 (2011) [arXiv:1107.1252 [hep-ph]].
 - [30] E. Iancu, K. Itakura, L. McLerran, Nucl. Phys. **A708**, 327-352 (2002) [arXiv:hep-ph/0203137].
 - [31] S. Munier and R. Peschanski, Phys. Rev. Lett. **91** (2003) 232001 [arXiv:hep-ph/0309177]; Phys. Rev. D **69** (2004) 034008 [arXiv:hep-ph/0310357].
 - [32] M. Braun, Eur. Phys. J. **C16**, 337-347 (2000) [arXiv:hep-ph/0001268].

- [33] A. H. Mueller and D. N. Triantafyllopoulos, Nucl. Phys. B **640**, 331 (2002) [arXiv:hep-ph/0205167].
- [34] D. N. Triantafyllopoulos, Nucl. Phys. B **648**, 293 (2003) [arXiv:hep-ph/0209121].
- [35] J. L. Albacete, N. Armesto, J. G. Milhano and C. A. Salgado, Phys. Rev. D **80**, 034031 (2009) [arXiv:0902.1112 [hep-ph]].
- [36] J. L. Albacete, N. Armesto, J. G. Milhano, P. Quiroga-Arias and C. A. Salgado, Eur. Phys. J. C **71**, 1705 (2011) [arXiv:1012.4408 [hep-ph]].

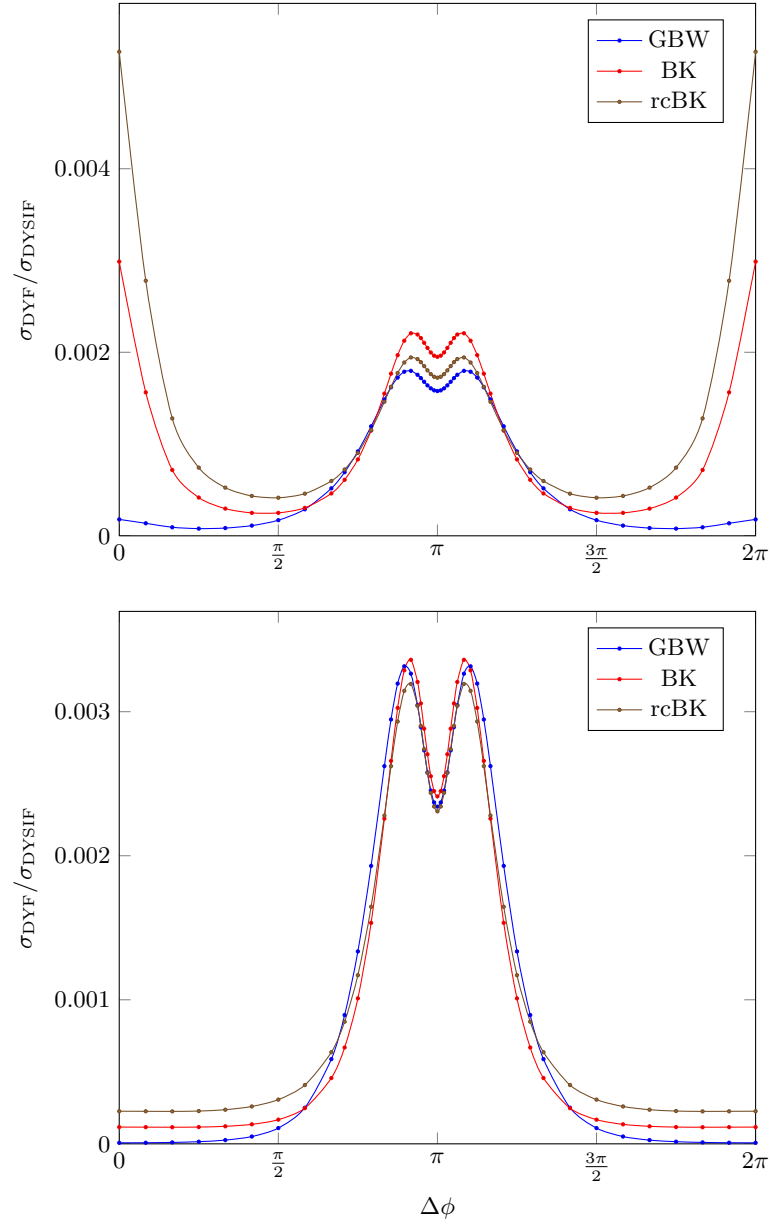


FIG. 5: The angular correlations between the virtual photons and pions at RHIC, at medium rapidity, $Y_\gamma = Y_\pi = 2.5$. The upper graph shows the correlation for a virtual photon mass of $M = 0.5 \text{ GeV}$, and the lower one, for $M = 4 \text{ GeV}$. In each case, the three curves for GBW, fixed coupling BK, and running coupling BK, exhibit basically the same double-peak structure around $\Delta\phi = \pi$, but they show differing behavior near $\Delta\phi = 0, 2\pi$, the near side correlation. This relates to the large- k^2 behavior of the corresponding gluon distributions.

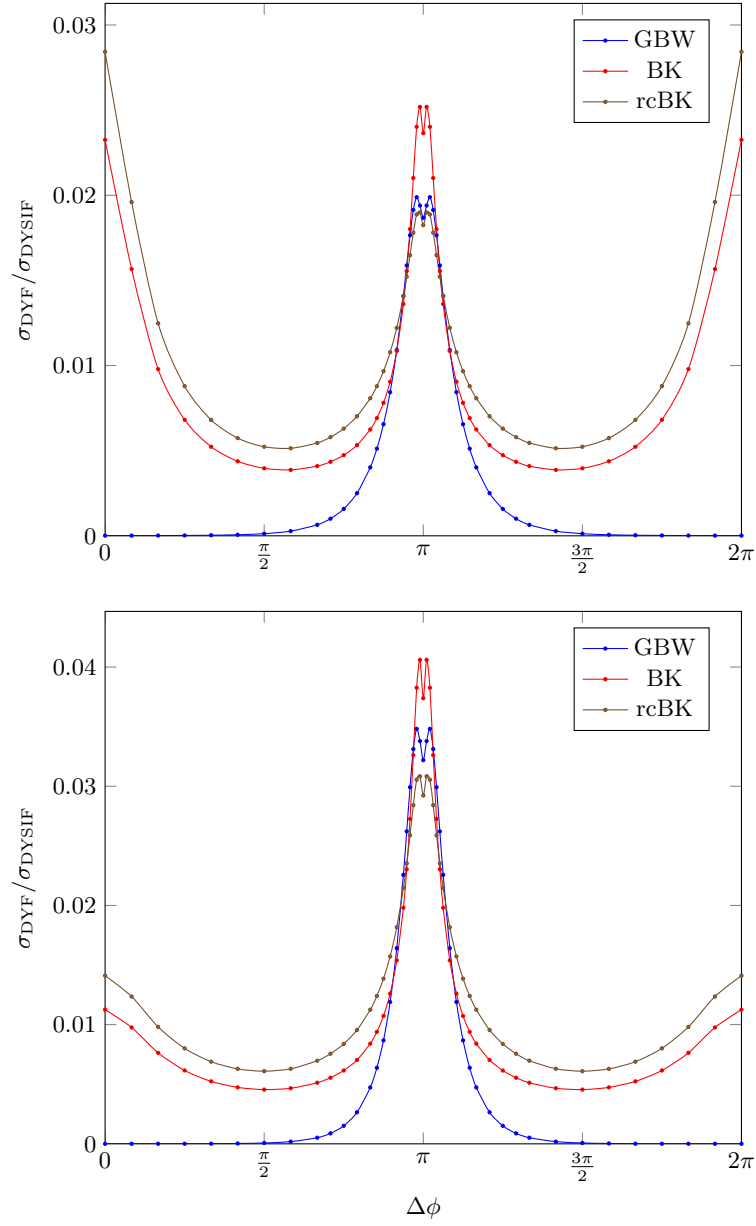


FIG. 6: The virtual photon-pion angular correlations at LHC at rapidity $Y_\gamma = Y_\pi = 4$. The upper and lower graphs show $M = 4 \text{ GeV}$ and $M = 8 \text{ GeV}$, respectively. As in figure 5, the key difference is in the near side correlation, arising due to differences in the high-momentum region of the gluon distribution.